(2+1)-dimensional X-shaped localized waves

Ioannis M. Besieris*
The Bradley Department of Electrical and Computer Engineering, Virginia Polytechnic Institute and State University, Blacksburg, Virginia 24060, USA

Amr M. Shaarawi
Department of Physics, The American University of Cairo, P.O. Box 2511, Cairo 11511, Egypt
(Received 16 July 2005; published 29 November 2005)

A hybrid spectral superposition method is presented that allows a smooth transition between two seemingly distinct classes of localized wave solutions to the homogeneous scalar wave equation in free space; specifically, luminal or focus wave modes, and superluminal or X waves. This representation, which is based on superpositions of products of forward plane waves moving at a fixed speed $v>c$ and backward plane waves moving at the speed c, is used to construct a large class of finite-energy superluminal-type X-shaped localized waves. The latter are characterized by arbitrarily high-frequency bands and are suitable for applications in the microwave and optical regime. In the limiting case $v\to c$, one recaptures the well-known focus wave mode-type localized wave solutions. A modified hybrid spectral representation, based on superpositions of products of forward plane waves moving at a fixed speed c and backward plane waves moving at the speed $v>c$, allows in the limit $v\to c$ a smooth transition from superluminal localized waves to paraxial luminal pulsed beams. Although the proposed methods are applicable to a $(n+1)$-dimensional, $n\geqslant 2$, scalar wave equation, the discussion will be limited to the case $n=2$ for simplicity; also, so that comparisons can be made to related recent results in the literature.

DOI: 10.1103/PhysRevE.72.056612 PACS number(s): 03.50.De, 41.20.−q, 42.25.−p

I. INTRODUCTION

In recent years, there has been increasing interest in novel classes of spatiotemporally localized solutions to various hyperbolic equations governing acoustic, electromagnetic, and quantum wave phenomena. The bulk of the research along these lines has been performed in connection with the basic formulation, generation, guidance, propagation, scattering, and diffraction of three distinct types of acoustic and electromagnetic localized waves (LWs) in free space: *luminal*, or focus wave modes (FWMs), *superluminal*, or X waves (XWs), and *subluminal* (see [1–7] for pertinent review literature). Some work, however, has been done in the areas of propagation of LWs in dispersive (see [8] and references therein) and nonlinear (see [9] and references therein) media. In general, both linear and nonlinear LW pulses exhibit distinct advantages in their performance in comparison to conventional quasimonochromatic signals. Their spatiotemporal localization and extended field depths render them very useful in diverse physical applications, such as secure signaling, laser-induced particle acceleration, ultrafast microscopy, high resolution imaging, tissue characterization, photodynamic therapy, etc.

The *simplest* spatiotemporally localized X-shaped pulse is the "pure" X wave solution,

$$\psi(\rho,z,t)=\frac{1}{\sqrt{\rho^2+[a_1+i\gamma(z-vt)]^2}};\quad \rho\equiv\sqrt{x^2+y^2};$$

$$\gamma\equiv\frac{1}{\sqrt{(v/c)^2-1}} \tag{1.1}$$

to the (3+1)-dimensional homogeneous scalar wave equation in free space. In this expression, $v>c$ and a_1 is an arbitrary positive parameter. This solution, which was introduced by Lu and Greenleaf [10] in 1992, is an infinite-energy wave packet propagating without distortion along the z direction with the superluminal speed v. Analogous spatiotemporally localized X waves can be found in higher spatial dimensions; specifically,

$$\psi(x_1,x_2,\ldots x_n,t)=\left(\sum_{j=1}^{n-1}x_j^2+[a_1+i\gamma(x_n-vt)]^2\right)^{(2-n)/2};\ n\geqslant 3. \tag{1.2}$$

It is well known [11], however, that no such solution is possible for the (2+1)-D scalar wave equation

$$\left(\frac{\partial^2}{\partial x^2}+\frac{\partial^2}{\partial z^2}-\frac{1}{c^2}\frac{\partial^2}{\partial t^2}\right)\psi(x,z,t)=0. \tag{1.3}$$

A proof of this statement can be given as follows. Introducing the new variable $\zeta=z-vt$, $v>c$, Eq. (1.3) can be rewritten as

$$\left(\frac{\partial^2}{\partial x^2}-\frac{1}{\gamma^2}\frac{\partial^2}{\partial \zeta^2}\right)\psi(x,\zeta)=0, \tag{1.4}$$

a general solution of which is given by $\psi(x,\zeta)=\psi_1(x-\gamma\zeta)+\psi_2(x+\gamma\zeta)$. The latter is nonlocalized. At $z=0$, in particular, $\psi(x,0,t)=\psi_1(x+\gamma vt)+\psi_2(x-\gamma vt)$ consists of a sum of two

*Electronic address: besieris@vt.edu

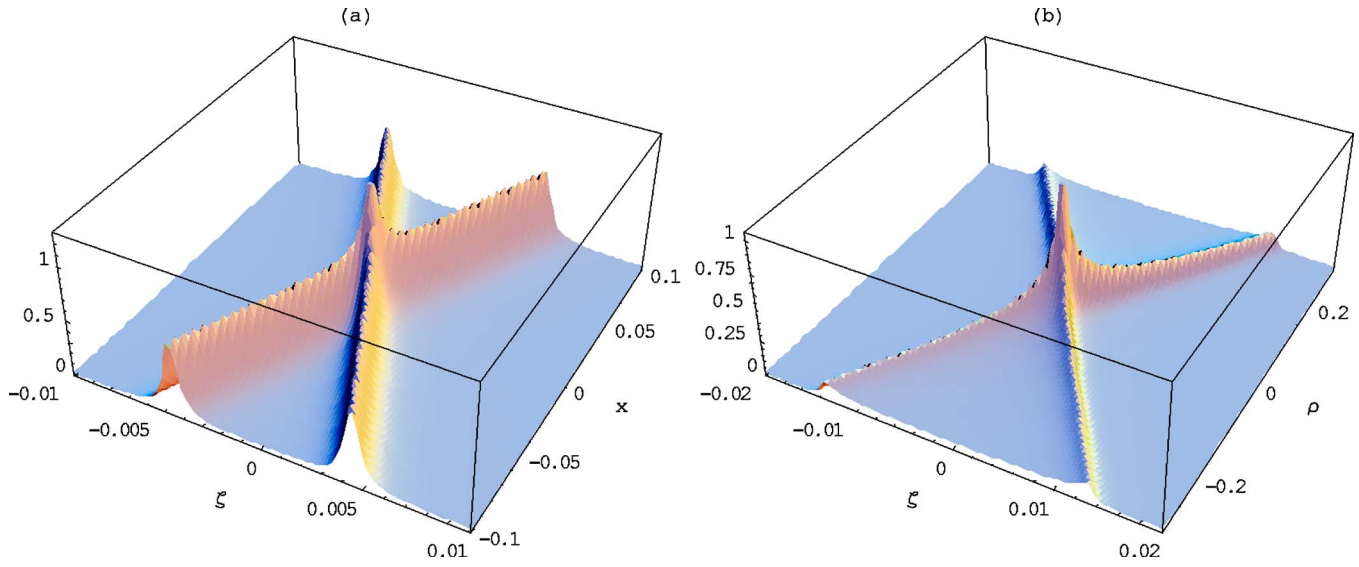

FIG. 1. (Color online) (a) Unlocalized Ciattoni-Di Porto (2+1)-D wave packet: $\mathrm{Re}\{\psi_0(x,\zeta)\}$ vs x,ζ. (b) Localized (3+1)-D X wave: $\mathrm{Re}\{\psi(\rho,\zeta)\}$ vs ρ,ζ; Parameter values: $a_1=10^{-2}$ m, $\nu=1.00c$.

distortionless wave solutions traveling along the positive and negative x directions with speed $\gamma\nu$.

In their recent work on X-shaped solutions to the (2+1)-D scalar wave equation, Ciattoni and Di Porto [12] presented the fundamental solution

$$\psi_0(x,\zeta)=\frac{2(a_1+i\gamma\zeta)}{x^2+(a_1+i\gamma\zeta)^2}, \tag{1.5}$$

as the (2+1)-D analog of the (3+1)-D X wave in Eq. (1.1). The expression above can be brought into the form

$$\psi_0(x,\zeta)=\frac{1}{a_1+i(x+\gamma\zeta)}+\frac{1}{a_1-i(x-\gamma\zeta)}. \tag{1.6}$$

Based on the discussion above, this structure is *diffractionless* but *not localized*. This is evident in Fig. 1(a), which shows a surface plot of $\mathrm{Re}\{\psi_0(x,\zeta)\}$. In contrast, Fig. 1(b) is a surface plot of the real part of the localized (3+1)-D X wave given in Eq. (1.1). For both plots, $\nu=1.001c$ and $a_1=10^{-2}$ m.

Our main aim in this paper is to examine the possibility of diffractionless (infinite energy) and limited-diffraction (finite energy) spatiotemporally localized X-shaped solutions to the (2+1)-D scalar wave equation (1.3). It will be established that such solutions do exist; in contradistinction, however, to the pure (3+1)-D X wave pulse in Eq. (1.1), they involve two fixed speeds: the superluminal speed ν and the subluminal speed c^2/ν.

II. (2+1)-D X-SHAPED SOLUTIONS TO THE SCALAR WAVE EQUATION

A. Superluminal spectral representation

A general solution to the (2+1)-D scalar wave equation (1.3) can be expressed in terms of the *superluminal spectral representation* [3],

$$\psi(x,z,t)=\int_{-\infty}^{\infty}d\lambda\int_{-\infty}^{\infty}dk_x\exp\left[i\lambda\gamma\frac{\nu}{c}\left(z-\frac{c^2}{\nu}t\right)\right]\times\exp[-i\gamma(z-\nu t)\sqrt{k_x^2+\lambda^2}]\exp(-ik_x x)\psi(k_x,\lambda), \tag{2.1}$$

based on the invariance of the scalar wave equation under a generalized Lorentz transformation. This representation, which consists of superpositions of products of forward plane waves moving at a fixed speed $\nu>c$ and backward plane waves moving at the subluminal speed c^2/ν, is the most natural setting for deriving all X-shaped localized solutions to the scalar wave equation. Unfortunately, one cannot use Eq. (2.1) to examine the limiting condition $\nu\to c$ due to the presence of γ. For this reason, it will be prove convenient in the following discussion to transform Eq. (2.1) into a new spectral representation involving the fixed speeds ν and c.

B. Hybrid spectral representation

In Eq. (2.1), the following transformations are made from the wave numbers (λ,k_x) to the new wave numbers (α,β):

$$-\gamma\sqrt{\lambda^2+k_x^2}+\gamma\lambda(c/\nu)=\alpha+\beta(c/\nu);$$

$$-\gamma\sqrt{\lambda^2+k_x^2}+\gamma\lambda(\nu/c)=\alpha-\beta. \tag{2.2}$$

One, then, obtains

$$\psi(x,z,t)=\int_{-\infty}^{\infty}d\alpha\int_{-\infty}^{\infty}d\beta\,e^{-i\alpha(z-\nu t)}e^{i\beta(z+ct)}\times\exp\left[-ix\sqrt{\frac{\alpha^2}{\gamma^2}+2\left(1+\frac{\nu}{c}\right)\alpha\beta}\right]\psi(\alpha,\beta). \tag{2.3}$$

This *hybrid spectral representation* is based on superposi-

tions of products of forward plane waves moving at a fixed speed $v>c$ and backward plane waves moving at the speed c. In the limiting case $v\to c$, one recaptures a variant of the (2+1)-D *luminal bidirectional spectral representation* [13] that leads to well-known FWM localized wave solutions.

C. (2+1)-D focus X waves

It follows from Eq. (2.3) that both

$$\psi_c(x,z,t)=\int_{-\infty}^{\infty}d\alpha\int_{-\infty}^{\infty}d\beta\, e^{-i\alpha(z-vt)}e^{i\beta(z+ct)}\times\cos\left[x\sqrt{\frac{\alpha^2}{\gamma^2}+2\left(1+\frac{v}{c}\right)\alpha\beta}\right]\psi_c(\alpha,\beta),$$

$$\psi_s(x,z,t)=\int_{-\infty}^{\infty}d\alpha\int_{-\infty}^{\infty}d\beta\, e^{-i\alpha(z-vt)}e^{i\beta(z+ct)}\times\sin\left[x\sqrt{\frac{\alpha^2}{\gamma^2}+2\left(1+\frac{v}{c}\right)\alpha\beta}\right]\psi_s(\alpha,\beta), \tag{2.4}$$

are solutions to the (2+1)-D scalar wave equation. In the sequel, only the former will be considered in detail. The spectrum in Eq. (2.4a) is chosen as follows:

$$\psi_c(\alpha,\beta)=\sqrt{2/\pi}\,\delta(\beta-\beta')\exp(-a_0\alpha)\times\left[\alpha+2\gamma^2\left(1+\frac{v}{c}\right)\beta\right]^{-1/2}H(\alpha)H(\beta). \tag{2.5}$$

Here, $\delta(\cdot)$ denotes the Dirac delta function, $H(\cdot)$ is the Heaviside unit step function, and a_0 ad β' are arbitrary positive parameters. With the introduction of this spectrum, the integration over β can be carried out very simply and the remaining integration over α yields (see [14], p. 249)

$$\psi_c(x,z,t;\beta')=\exp[i\beta'(z+ct)]\times\exp\left[\gamma^2\left(1+\frac{v}{c}\right)\beta'[a_0+i(z-vt)]\right]\times\frac{\sqrt{a_0+i(z-vt)+\sqrt{(x/\gamma)^2+[a_0+i(z-vt)]^2}}}{\sqrt{(x/\gamma)^2+[a_0+i(z-vt)]^2}}\times\exp\left[-\gamma^2\left(1+\frac{v}{c}\right)\times\beta'\sqrt{(x/\gamma)^2+[a_0+i(z-vt)]^2}\right]. \tag{2.6}$$

A number of observations can be made regarding this solution. For $\beta'=0$, one obtains the restricted exact solution

$$\psi(x,z,t)=\frac{\sqrt{a_0+i(z-vt)+\sqrt{(x/\gamma)^2+[a_0+i(z-vt)]^2}}}{\sqrt{(x/\gamma)^2+[a_0+i(z-vt)]^2}}=\sqrt{\frac{a_0+i(z-vt)}{(x/\gamma)^2+[a_0+i(z-vt)]^2}+\frac{1}{\sqrt{(x/\gamma)^2+[a_0+i(z-vt)]^2}}}, \tag{2.7}$$

which involves only the speed v. The second part underneath the square root in (2.7b) is localized transversely and axially, but the first part is not. As a consequence, the entire solution is distortionless but *unlocalized* as expected from the previous discussion. For $\beta'\neq 0$, the solution given in Eq. (2.6) is spatiotemporally localized due to the presence of the third exponential term.

In order to understand the nature of $\psi_c(x,z,t;\beta')$ in (2.6) more completely, it should be noted that carrying out carefully the limit $v\to c$ yields the luminal solution

$$\psi_c(x,z,t;\beta')\Big|_{v\to c}\to\psi_{FWM}(x,z,t;\beta')=\frac{\exp[i\beta'(z+ct)]}{\sqrt{a_0+i(z-ct)}}\times\exp\left(-\beta'\frac{x^2}{a_0+i(z-ct)}\right), \tag{2.8}$$

modulo a constant multiplier term. This is the (2+1)-D version of the FWM originally introduced by Brittingham in 1983 [15]. The wave function consists of an envelope traveling along the positive z direction with speed c, modulated by a plane wave moving in the negative z direction with the same speed. The entire wave packet sustains only local deformations; more precisely, it regenerates for values of t equal to $n\pi/\beta$, n being an integer. The FWM is physically unrealizable because it contains infinite energy.

For the reasons given above, the solution $\psi_c(x,z,t;\beta')$ in Eq. (2.6) is referred to as a (2+1)-D *focus X wave* (FXW). [This nomenclature was introduced in Ref. [3] for an analogous solution to the (3+1)-D scalar wave equation.] For $v>c$, it is an X-shaped, transversely and axially localized pulse, except that its highly focused central region has a tight exponential localization, analogous to that of a FWM. As the speed v approaches c from above, the (2+1)-D focus X wave acquires the properties of the luminal (2+1)-D FWM given in Eq. (2.8). The main purpose of the hybrid form of $\psi_c(x,z,t;\beta')$ in Eq. (2.6) is to allow for such a smooth transition. An additional advantage of the hybrid form is that it obviates the presence of backward wave components moving at the luminal speed c. To make the last point clearer, the first two exponential terms in Eq. (2.6) can be combined in order to yield the following alternative form of the (2+1)-D focus X wave:

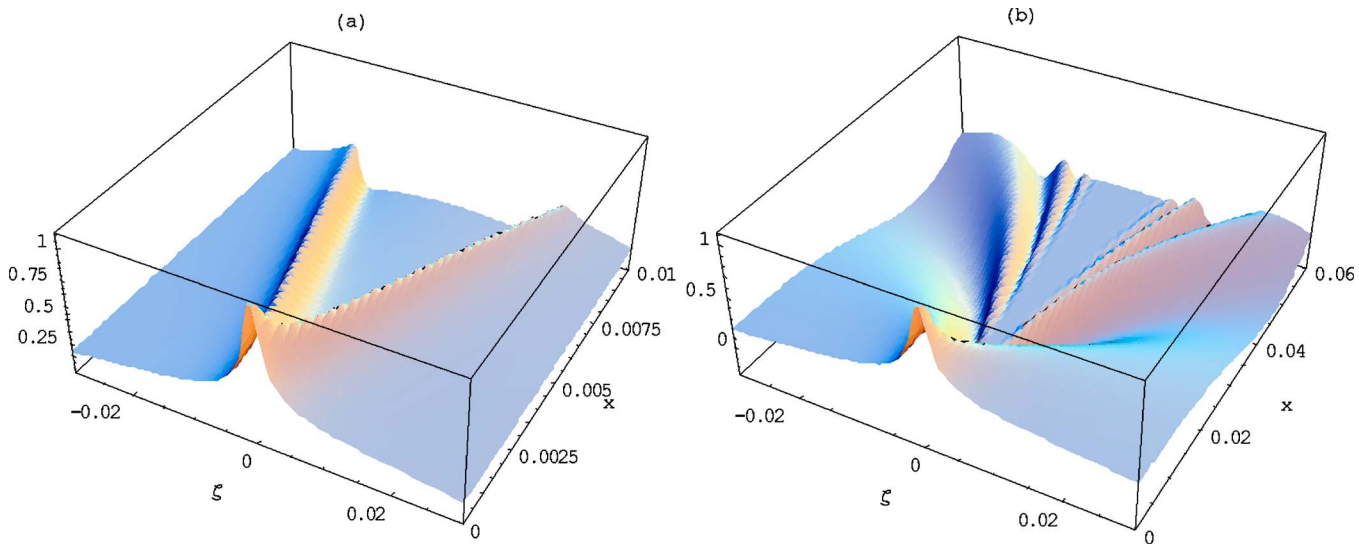

FIG. 2. (Color online) (a) (2+1)-D focus X wave: $\mathrm{Re}\{\psi_{FXW}(x,\zeta;\beta')\}$ vs x,ζ, with parameter values $\nu=2c$, $\beta'=40\ \mathrm{m}^{-1}$, and $a_0=10^{-3}$ m. (b) Transition to a (2+1)-D focus wave mode: $\mathrm{Re}\{\psi_{FXW}(x,\zeta;\beta')\}$ vs x,ζ, with parameter values $\nu=1.000\,000\,1c$, $\beta'=40\ \mathrm{m}^{-1}$, and $a_0=10^{-3}$ m.

$$\psi_c(x,z,t;\beta') = \exp\left[\gamma^2\left(1+\frac{\nu}{c}\right)\beta' a_0\right] \times \exp\left[i\beta'(1-c/\nu)^{-1}\left(z-\frac{c^2}{\nu}t\right)\right] \times \frac{\sqrt{a_0+i(z-\nu t)+\sqrt{(x/\gamma)^2+[a_0+i(z-\nu t)]^2}}}{\sqrt{(x/\gamma)^2+[a_0+i(z-\nu t)]^2}} \times \exp\left[-\gamma^2\left(1+\frac{\nu}{c}\right) \times \beta'\sqrt{(x/\gamma)^2+[a_0+i(z-\nu t)]^2}\right]. \quad (2.9)$$

This expression seems to be *unidirectional* in the sense that it consists of an envelope traveling in the positive z direction with the superluminal speed ν, multiplied by a plane wave also moving in the positive z direction, however, at the subluminal speed c^2/ν. Of course, the unidirectionality of the wave packet is only apparent, as it is made clear in the hybrid form.

The modulus of (2+1)-D focus X wave, in either the hybrid form given in Eq. (2.6) or the superluminal form in Eq. (2.9), depends only of x and $z-\nu t$. As a consequence, it moves along the positive z direction with a superluminal speed ν rigidly, without sustaining any distortion. This means that $\psi_c(x,z,t;\beta')$ contains infinite energy. The real part of this function regenerates periodically along the z direction. The regeneration period equals $\nu t=(2\pi n)/[\beta'(1+(c/\nu)]$, where n is an integer. Figure 2(a) shows a surface plot of $\mathrm{Re}\{\psi_c(x,z,t;\beta')\}$ for the parameter values $\beta'=40m^{-1}$, $a_0=10^{-3}m$ and $\nu=2c$. The X shape of the (2+1)-D focus X wave is clearly evident. The transition of the wave packet into a (2+1)-D FWM is depicted in Fig. 2(b), where the values of β' and a_0 have been kept the same but $\nu=1.000\,000\,001c$.

D. (2+1)-D finite-energy X-shaped localized waves

Let $\omega'\equiv\beta'/c(\mathrm{rad/s})$ and consider the superposition

$$\psi_c(x,z,t)=\frac{1}{\pi}\int_0^\infty d\omega'\ \psi_c(x,z,t;\omega')G(\omega'), \quad (2.10)$$

where $\psi_c(x,z,t;\beta'=\omega'/c)$ is the (2+1)-D FXW solution given in Eq. (2.6). If $\hat{g}(t)$ denotes the complex analytic signal corresponding to the temporal spectrum $G(\omega')$, one obtains the finite-energy (2+1)-D X-shaped localized wave solution

$$\psi_c(x,z,t)=\frac{\sqrt{a_0+i(z-\nu t)+\sqrt{(x/\gamma)^2+[a_0+i(z-\nu t)]^2}}}{\sqrt{(x/\gamma)^2+[a_0+i(z-\nu t)]^2}} \times \hat{g}\left[\left(t+\frac{z}{c}\right)-i\frac{1}{c}\gamma^2\left(1+\frac{\nu}{c}\right)[a_0+i(z-\nu t) - \sqrt{(x/\gamma)^2+[a_0+i(z-\nu t)]^2}]\right]. \quad (2.11)$$

As an illustrative example, consider the spectrum

$$G(\omega')=(\omega'-\omega_0)^q\exp[-a_1(\omega'-\omega_0)]H(\omega'-\omega_0), \quad (2.12)$$

with a_1, $\omega_0>0$ and $q>-1$. The complex analytic signal associated with this spectrum is given explicitly as follows ([14], p. 137):

$$\hat{g}(t)=\Gamma(q+1)\exp[-\omega_0(a_1-it)](a_1-it)^{-q-1}. \quad (2.13)$$

When this result is used in conjunction with Eq. (2.11), one obtains

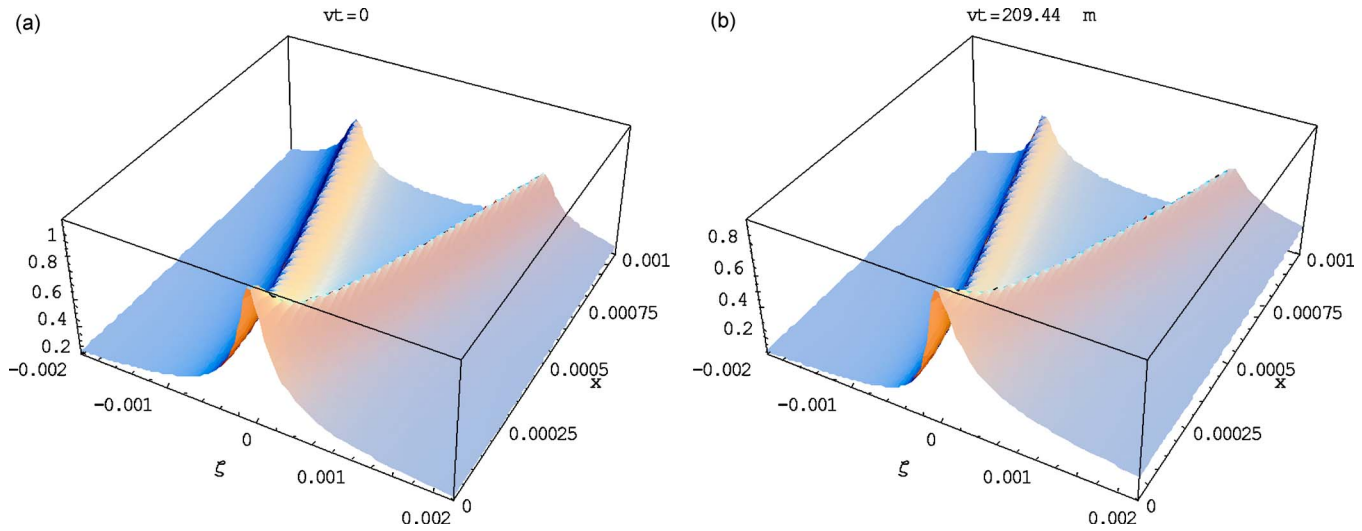

FIG. 3. (Color online) (2+1)-D modified focus X wave: $\mathrm{Re}\{\psi_{MFXW}(x,\zeta;\nu t)\}$ vs x,ζ, with $\nu=1.5c$, $a_0\gamma=10^{-4}$ m, $a_1c=10^3$ m, $q=0$ and $\omega_0=60c$ (rad/s). (a) $n=0(\nu t=0)$; (b) $n=5000(\nu t=209.44$ m).

$$\psi_c(x,z,t)=\Gamma(q+1)\times\frac{\sqrt{a_0+i(z-\nu t)+\sqrt{(x/\gamma)^2+[a_0+i(z-\nu t)]^2}}}{\sqrt{(x/\gamma)^2+[a_0+i(z-\nu t)]^2}}\times\frac{1}{p^{q+1}}\exp(-\omega_0 p);$$

$$p\equiv a_1-i\left(t+\frac{z}{c}\right)-\frac{1}{c}\gamma^2\left(1+\frac{\nu}{c}\right)\{a_0+i(z-\nu t)-\sqrt{(x/\gamma)^2+[a_0+i(z-\nu t)]^2}\}. \quad (2.14)$$

It should be noted that carrying out carefully the limit $\nu\to c$ yields the luminal solution

$$\psi_c(x,z,t)\Big|_{\nu\to c}\to\psi_{MPS}(x,z,t)=\frac{\exp[i(\omega_0/c)(z+ct)]}{\sqrt{a_0+i(z-ct)}}\times\exp\left(-\frac{\omega_0}{c}\frac{x^2}{a_0+i(z-ct)}\right)\times\left(a_2-i(z+ct)+\frac{x^2}{a_0+i(z-ct)}\right)^{-q-1};$$

$$a_2\equiv a_1c. \quad (2.15)$$

modulo a constant multiplier term. This is the (2+1)-D version of the finite-energy modified power spectrum (MPS) pulse originally derived by Ziolkowski [1] from a superposition of pure FWMs. For this reason, the solution $\psi_c(x,z,t)$ in (2.14) is referred to as a (2+1)-D *modified focus X wave* (MFXW). For $\nu>c$, it is an X-shaped, transversely and axially localized pulse, except that its highly focused central region has a tight exponential localization, analogous to that of a MPS pulse.

It should be noted that the presence of a superluminal speed in the finite energy MFXW solution in Eq. (2.14) does not contradict relativity. If the parameters are chosen so that the solution contains mostly forward propagating components, the pulse moves superluminally with almost no distortion up to a certain distance z_d, and then it slows down to a luminal speed c, with significant accompanying distortion. Although the peak of the pulse does move superluminally up to z_d, it is not causally related at two distinct ranges z_1, $z_2\in[0,z_d)$. Thus, no information can be transferred superluminally from z_1 to z_2. The physical significance of the (2+1)-D MFXW is due to its spatiotemporal localization.

Figure 3 shows surface plots of the real part of the (2+1)-D MFXW for the parameter values $\nu=1.5c$, $a_0=10^{-4}/\gamma(\mathrm{m})$, $q=0$, $a_1=10^3/c(\mathrm{s})$, $\omega_0=60c(\mathrm{rad/s})$, and different values of $\nu t=(2\pi n)/[(\omega_0/c)(1+(c/\nu)]$ at which the wave packet is expected to partially regenerate. The X shape of the (2+1)-D MFXW is clearly evident. The finite energy of the pulse causes a distortion of the pulse shape at the range $\nu t\approx 209.44(\mathrm{m})$ for the given parameters. The transition of the wave packet into a (2+1)-D MPS pulse is depicted in Fig. 4, for the parameter values $\nu=1.000\,01c$, $a_0=10^{-2}/\gamma(\mathrm{m})$, $a_1=10^3/c(\mathrm{s})$, $q=0$, and $\omega_0=3c(\mathrm{rad/s})$, again for different ranges $\nu t=(2\pi n)/[(\omega_0/c)(1+(c/\nu)]$ at which the wave packet is expected to partially regenerate.

III. (2+1)D SPLASH MODES AND FOCUSED PULSED BEAMS

Recent advances in ultrafast optical technology have made possible the generation of single-cycle and half-cycle electromagnetic pulses of subpicosecond temporal duration. These pulses have center frequencies in the terahertz range and spectra that extend from zero to several terahertz. This extraordinary large bandwidth results in significant temporal reshaping of focused terahertz pulses, even when they propagate through free space. An analysis of this diffraction-induced pulse reshaping is usually carried out numerically or analytically within the framework of the paraxial approximation. A modified hybrid spectral representation will be introduced in this section that allows an exact analysis of a large class of finite-energy focused pulsed beams.

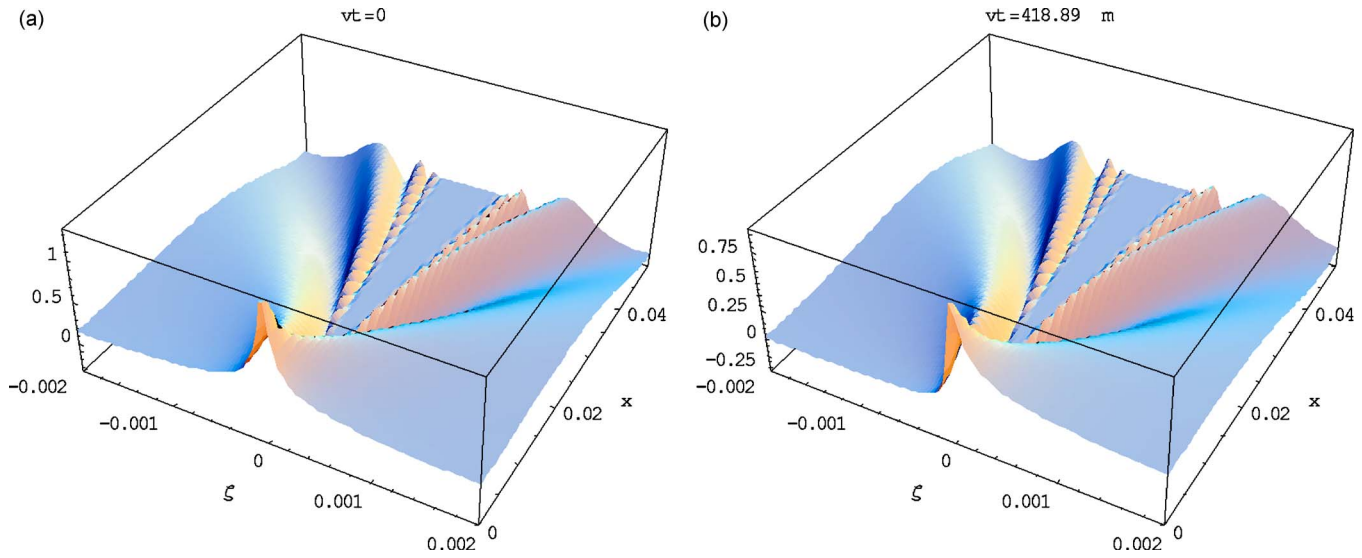

FIG. 4. (Color online) Transition to a (2+1)-D modified power spectrum pulse: $\mathrm{Re}\{\psi_{MFXW}(x,\zeta;\nu t)\}$ vs x,ζ, with $\nu=1.000\,01c$, $a_0\gamma=10^{-2}$ m, $a_1c=10^3$ m, $q=0$, and $\omega_0=3c$ (rad/s). (a) $n=0(\nu t=0)$; (b) $n=400(\nu t=418.89$ m).

A. Modified hybrid spectral representation

In the superluminal spectral representation given in Eq. (2.1), the following transformations are made from the wave numbers (λ,k_x) to the new wave numbers (α,β):

$$-\gamma\sqrt{k_x^2+\lambda^2}+\lambda\gamma(c/\nu)=\alpha(c/\nu)+\beta;$$

$$-\gamma\sqrt{k_x^2+\lambda^2}+\lambda\gamma(\nu/c)=\alpha-\beta. \tag{3.1}$$

One then obtains

$$\psi(x,z,t)=\int_{-\infty}^{\infty}d\alpha\int_{-\infty}^{\infty}d\beta\,e^{-i\alpha(z-ct)}e^{i\beta(z+\nu t)}\times\exp\left[-ix\sqrt{\frac{\beta^2}{\gamma^2}+2\left(1+\frac{\nu}{c}\right)\alpha\beta}\right]\psi(\alpha,\beta). \tag{3.2}$$

This *modified hybrid spectral representation* is based on superpositions of products of forward plane waves moving at a fixed speed c and backward plane waves moving at the speed $\nu>c$. This representation allows a smooth transition from superluminal localized waves to *pulsed beams*.

B. (2+1)-D splash modes and focused pulsed beams

Proceeding along the lines followed in Sec. II, it can be established that a broad class of (2+1)-D superluminal-type solutions based on the modified hybrid spectral representation is given by

$$\psi(x,z,t)=\frac{\sqrt{a_2-i(z+\nu t)+\sqrt{(x/\gamma)^2+[a_2-i(z+\nu t)]^2}}}{\sqrt{(x/\gamma)^2+[a_2-i(z+\nu t)]^2}}\times f[\theta(x,z,t)];$$

$$\theta(x,z,t)=-i(z-ct)+\left(\frac{\nu}{c}+1\right)\gamma^2\{a_2-i(z+\nu t)-\sqrt{(x/\gamma)^2+[a_2-i(z+\nu t)]^2}\};$$

$$\gamma=\frac{1}{\sqrt{(\nu/c)^2-1}};\quad \nu>c,\ a_2>0, \tag{3.3}$$

with $f(\cdot)$ essentially an arbitrary function. A specific solution of this type is the following:

$$\psi_{VFXW}(x,z,t;\alpha)=\frac{\sqrt{a_2-i(z+\nu t)+\sqrt{(x/\gamma)^2+[a_2-i(z+\nu t)]^2}}}{\sqrt{(x/\gamma)^2+[a_2-i(z+\nu t)]^2}}\times\exp\left[-i\alpha(z-ct)+\alpha\left(\frac{\nu}{c}+1\right)\times\gamma^2\{a_2-i(z+\nu t)-\sqrt{(x/\gamma)^2+[a_2-i(z+\nu t)]^2}\}\right]. \tag{3.4}$$

This is a variant of the (2+1)-D FXW in Eq. (2.6). In the limit $\nu\to c$, it reduces to a variant of the pure FWM; specifically,

$$\psi_{VFWM}(x,\zeta,\eta;\alpha)=\frac{1}{\sqrt{a_2-i\eta}}e^{-i\alpha\xi}\exp\left(-\alpha\frac{x^2}{a_2-i\eta}\right);$$

$$\xi=z-ct,\quad \eta=z+ct, \tag{3.5}$$

which is an exact solution to the (2+1)-D scalar wave equation (1.3). Superpositions of such solutions, viz.,

$$\psi_{SM/VFWM}(x,\zeta,\eta)=\int_0^{\infty}d\alpha\,G(\alpha)\psi_{VFWM}(x,z,t;\alpha) \tag{3.6}$$

are known as *luminal splash modes* [1]. Finite-energy *lumi-*

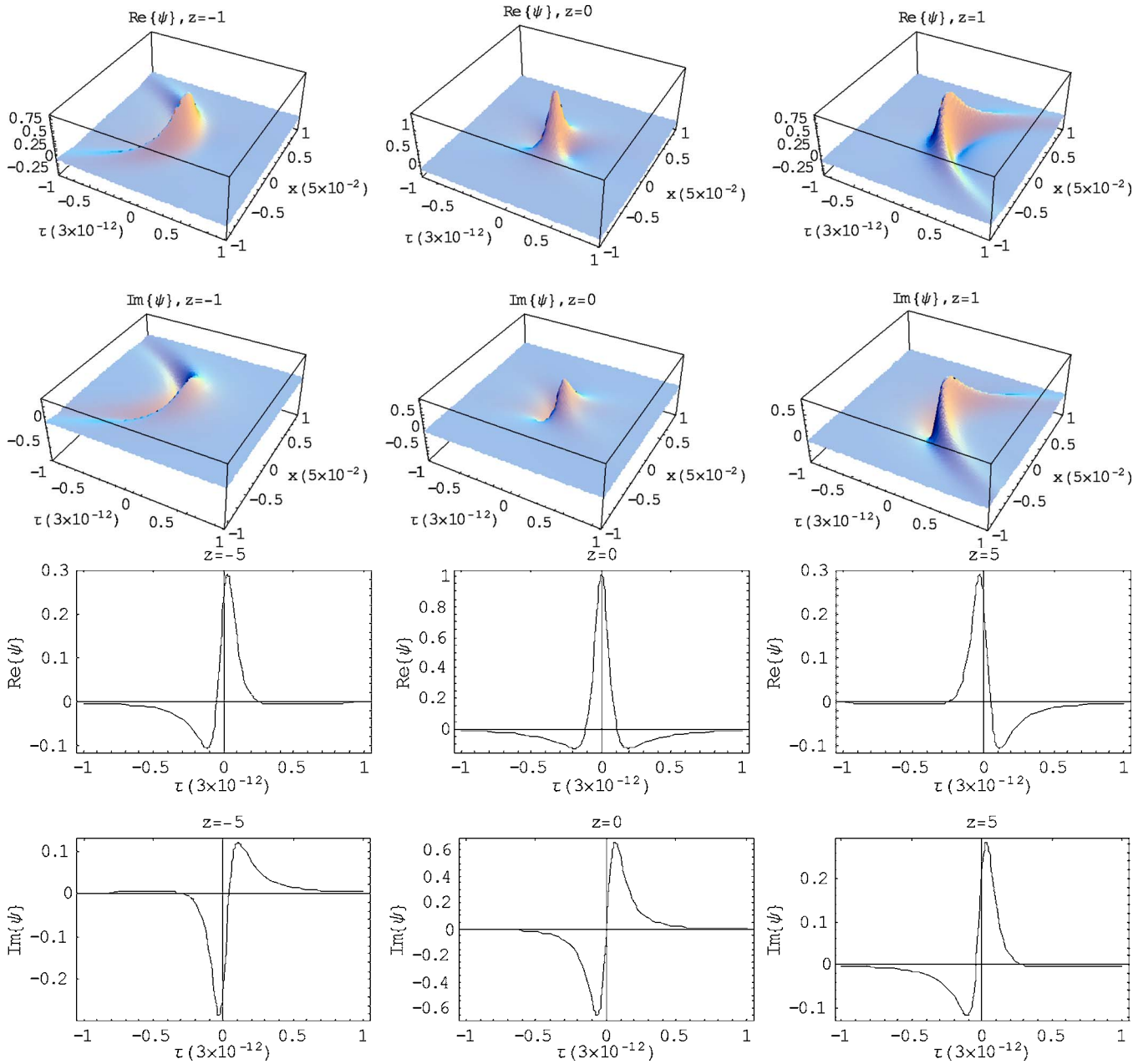

FIG. 5. (Color online) Spatiotemporal evolution of a focused pulsed beam from $z=-1$, through the focus ($z=0$) to $z=1$: (a) $\mathrm{Re}\{\psi_{FPB}(x,\tau;z)\}$ vs τ,x; (b) $\mathrm{Im}\{\psi_{FPB}(x,\tau;z)\}$ vs τ,x; $a_1=10^{-4}$ m, $a_2=1$ m, $q=1$, $b=2$ m^{-1} and $\nu=1.000\,000\,1c$. Temporal reshaping of a focused pulse from $z=-5$, through the focus ($z=0$) to $z=5$: (c) $\mathrm{Re}\{\psi_{FPB}(0,\tau;z)\}$ vs τ; (d) $\mathrm{Im}\{\psi_{FPB}(0,\tau;z)\}$ vs τ; $a_1=10^{-4}$ m, $a_2=1$ m, $q=1$, $b=2$ m^{-1} and $\nu=1.000\,000\,1c$.

nal pulsed beam solutions within the *paraxial approximation* can be obtained as follows:

$$\psi_{PB/VFWM}(x,z,t)=\int_0^\infty d\alpha\, G(\alpha)\psi_{VFWM}(x,\xi,\eta\to 2z;\alpha). \tag{3.7}$$

These solutions obey the pulsed beam equation [16,17]

$$\left(\frac{\partial^2}{\partial x^2}+2\frac{\partial^2}{\partial\xi\,\partial z}\right)\psi_{PB}(x,z,t)=0. \tag{3.8}$$

Analogously to Eq. (3.6), one obtains a new class of exact (2+1)-D finite-energy splash modes by means of the spectral synthesis

$$\psi_{SM/VFXW}(x,z,t)=\int_0^\infty d\alpha\, G(\alpha)\psi_{VFXW}(x,z,t;\alpha). \tag{3.9}$$

For an illustrative example, consider a spectrum analogous to that given in Eq. (2.12), viz.,

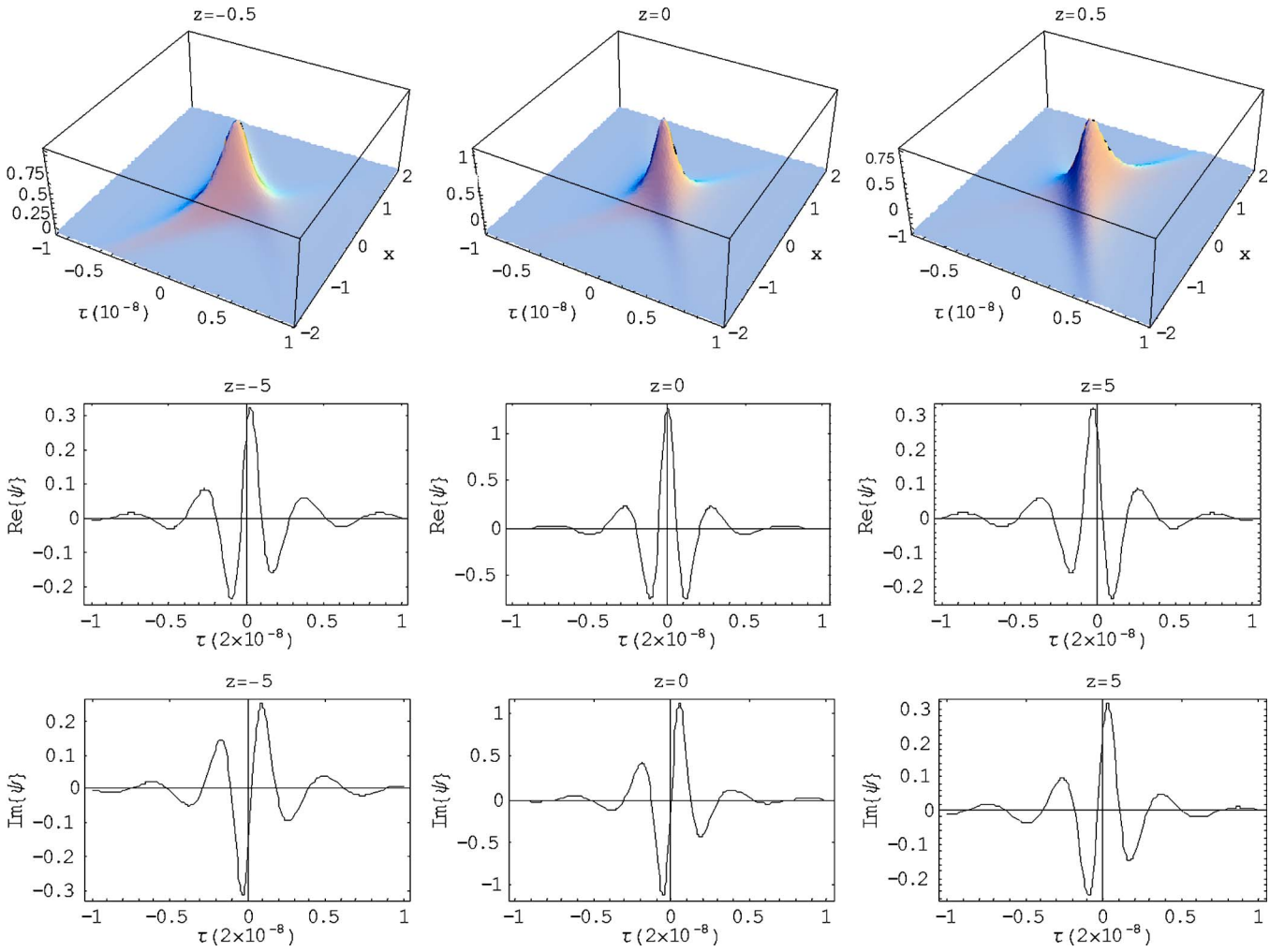

FIG. 6. (Color online) Spatiotemporal evolution of a nonparaxial splash mode pulse from $z=-1$, through the focus ($z=0$) to $z=1$: (a) $|\psi_{SM/VFXW}(x,\tau;z)|$ vs τ,x; (b) $\mathrm{Re}\{\psi_{SM/VFXW}(0,\tau;z)\}$ vs τ; (c) $\mathrm{Im}\{\psi_{SM/VFXW}(0,\tau;z)\}$ vs τ, The parameter values are as follows: $a_1=0.5$ m, $a_2=1$ m, $q=1$, $b=4$ m^{-1}, and $\nu=2c$.

$$G(\alpha)=(\alpha-b)^q\exp[-a_1(\alpha-b)]H(\alpha-b);\quad b>0. \tag{3.10}$$

The integration in Eq. (3.9) can be carried out explicitly, yielding the splash mode solution

$$\psi_{SM/VFXW}(x,z,t)=\Gamma(q+1)\frac{\sqrt{a_2-i(z+\nu t)+\sqrt{(x/\gamma)^2+[a_2-i(z+\nu t)]^2}}}{\sqrt{(x/\gamma)^2+a_2-i(z+\nu t)^2}}\frac{1}{P^{q+1}}\exp(-bP); \tag{3.11}$$

$$P\equiv a_1+i(z-ct)-\gamma^2\left(1+\frac{\nu}{c}\right)\{a_2-i(z+\nu t)-\sqrt{(x/\gamma)^2+[a_2-i(z+\nu t)]^2}\}.$$

In the limit $\nu\to c$, one obtains a luminal splash mode that is a variant of the MPS solution given in Eq. (2.15); specifically,

$$\psi_{SM/MPS}(x,z,t)=\frac{\exp[-ib(z-ct)]}{\sqrt{a_2-i(z+ct)}}\exp\left(-b\frac{x^2}{a_2-i(z+ct)}\right)\times\left(a_1+i(z-ct)+\frac{x^2}{a_2-i(z+ct)}\right)^{-q-1}. \tag{3.12}$$

If, in this expression, $z+ct$ is formally replaced by $2z$, one obtains a paraxial pulsed beam solution, viz.,

$$\psi_{PB/MPS}(x,z,t) = \frac{\exp[-ib(z-ct)]}{\sqrt{a_2 - i2z}} \exp\left(-b\frac{x^2}{a_2 - i2z}\right) \times \left(a_1 + i(z-ct) + \frac{x^2}{a_2 - i2z}\right)^{-q-1}, \tag{3.13}$$

governed by Eq. (3.8).

For values of ν very close to c and under the restriction $a_1 \; a_2$, the splash mode solution $\psi_{SM/VFXW}(x,z,t)$ given in Eq. (3.11) is indistinguishable from a paraxial focused pulsed beam obeying Eq. (3.8). The notation $\psi_{FPB}(x,z,t)$ will be used under these conditions. Figures 5(a) and 5(b) show, respectively, the spatiotemporal evolution of the real and imaginary parts of the solution $\psi_{FPB}(x,\tau;z)$ from the plane $z=-1$ m, passing through the focus ($z=0$), to the plane $z=1$ m, for the parameter values $a_1=10^{-4}$ m, $a_2=1$ m, $q=1$, $b=2$ m^{-1} and $\nu=1.000\,000\,1c$. One clearly observes the curved phase fronts, the polarity reversal, and temporal reshaping as the wave packet evolves through the focus. Figures 5(c) and 5(d) show, respectively, plots of $\mathrm{Re}\{\psi_{FPB}(0,\tau;z)\}$ vs τ and $\mathrm{Im}\{\psi_{FPB}(0,\tau;z)\}$ vs τ for the same parameter values and three ranges z. In an analogous (3+1)-D situation, it is well known [18] that the symmetric real solution at $z=0$ evolves in the farfield into an inverted version of the antisymmetric imaginary solution at $z=0$. Furthermore, the antisymmetric imaginary solution at $z=0$ evolves in the farfield into the symmetric real solution. Such a transformation of the pulse temporal profile has been observed in terahertz experiments [19,20]. In the (2+1)-D problem under consideration, the results are slightly different. Specifically, the real solution at $z=0$ evolves into an inverted version of the imaginary solution at $z=-5$ m. On the other hand, the imaginary solution at $z=0$ evolves into the real solution at $z=-5$ m.

The spatiotemporal evolution of the modulus of the splash mode solution $\psi_{SM/VFXW}(x,z,t)$ given in Eq. (3.11) is depicted in Fig. 6(a) in a *nonparaxial* framework; specifically, for the parameter values $a_1=0.5$ m, $a_2=1$ m, $q=1$, $b=4$ m^{-1}, and $\nu=2c$. Figures 6(b) and 6(c) are plots of $\mathrm{Re}\{\psi_{SM/VFXW}(0,\tau;z)\}$ vs τ and $\mathrm{Im}\{\psi_{SM/VFXW}(0,\tau;z)\}$ vs τ, respectively, for the same parameter values.

IV. CONCLUDING REMARKS

A hybrid spectral representation method has been presented that allows a smooth transition between superluminal, or X waves, and luminal, or focus wave modes. The technique has been used to obtain both infinite energy (FXW) and finite energy (MFXW) transversely and axially localized pulse solutions to the (2+1)-D scalar wave equation. TE and TM FXW and MFXW solutions to Maxwell's equations can readily be derived using the scalar-valued solutions obtained in this paper as the z components of electric and magnetic Hertz potentials. The hybrid spectral representation method can be used to obtain FXW and MFXW localized pulse solutions to the $(n+1)$-D, $n \geqslant 3$, scalar wave equation. Also, it can be used to derive analogous solutions to hyperbolic equations (e.g., the Klein-Gordon equation) governing the wave propagation in media characterized by temporal dispersion.

A modified hybrid spectral representation method has also been presented that allows a smooth transition from superluminal localized waves to exact splash modes. Within the framework of a certain parametrization, the latter are rendered indistinguishable from the paraxial luminal pulsed beam solutions governed by the pulsed beam equation (3.8). The specific example given in Sec. III illustrates the diffraction-induced temporal reshaping and polarity reversal of extremely short (one-cycle) focused pulses.

[1] R. W. Ziolkowski, Phys. Rev. A **39**, 2005 (1989).
[2] R. W. Ziolkowski, I. M. Besieris, and A. M. Shaarawi, Proc. IEEE **79**, 1371 (1991).
[3] I. M. Besieris, M. Abdel-Rahman, A. M. Shaarawi, and A. Chatzipetros, Prog. Electromagn. Res. **19**, 1 (1998).
[4] E. Recami, Physica A **252**, 586 (1998).
[5] J. Salo, J. Fagerholm, A. T. Friberg, and M. M. Salomaa, Phys. Rev. E **62**, 4261 (2000).
[6] R. Grunwald, V. Kebbel, U. Griebner, U. Neumann, A. Kummrow, M. Rini, E. T. Nibbering, M. Piche, G. Rousseau, and M. Fortin, Phys. Rev. A **67**, 063820 (2003).
[7] P. Saari and K. Reivelt, Phys. Rev. E **68**, 036612 (2003).
[8] S. Longhi, Phys. Rev. E **68**, 066612 (2003).
[9] C. Conti, S. Trillo, P. Di Trapani, G. Valiulis, A. Piskarskas, O. Jedrkiewicz, and J. Trull, Phys. Rev. Lett. **90**, 170406 (2003).
[10] J. Y. Lu and J. F. Greenleaf, IEEE Trans. Ultrason. Ferroelectr. Freq. Control **39**, 19-31 (1992).
[11] J. Fagerholm, A. T. Friberg, J. Huttunen, D. P. Morgan, and M. M. Salomaa, Phys. Rev. E **54**, 4347 (1996).
[12] A. Ciattoni and P. Di Porto, Phys. Rev. E **69**, 056611 (2004).
[13] I. M. Besieris, A. M. Shaarawi, and R. W. Ziolkowski, J. Math. Phys. **30**, 1254 (1989).
[14] A. Erdelyi, Ed., *Tables of Integral Transforms* (McGraw-Hill, New York, 1954), Vol. I.
[15] J. N. Brittingham, J. Appl. Phys. **54**, 1179 (1983).
[16] E. Heyman, " IEEE Trans. Antennas Propag. **42**, 311 (1994).
[17] M. A. Porras, Phys. Rev. E **58**, 1086 (1998).
[18] S. Feng, H. G. Winful, and R. W. Hellwarth, Phys. Rev. E **59**, 4630 (1999).
[19] E. Budiarto, N.-W. Pu, S. Jeong, and J. Bokor, Opt. Lett. **23**, 213 (1998).
[20] M. T. Reiten, S. A. Harmon, and R. A. Cheville, J. Opt. Soc. Am. B **20**, 2215 (2003).